ELSEVIER

Polymer 43 (2002) 6901–6909

polymer

www.elsevier.com/locate/polymer

Tensile property and interfacial dewetting in the calcite filled HDPE, LDPE, and LLDPE composites

Sangmin Kwon[a], Kwang J. Kim[a], Hyun Kim[a], Patit P. Kundu[a], Tae J. Kim[b], Young K. Lee[b], Byung H. Lee[b], Soonja Choe[a,*]

[a]*Department of Chemical Engineering, Inha University, Inchon 402-751, South Korea*
[b]*Taedok Institute of Technology, SK Corporation, Taejon 305-370, South Korea*

Received 6 November 2000; accepted 10 May 2002

Abstract

Mechanical properties and complex melt viscosity of unfilled and the calcite (calcium carbonate: $CaCO_3$) filled high density polyethylene (HDPE), low density polyethylene (LDPE), and linear low density polyethylene (LLDPE) composites using dumbbell bar and film specimens are studied. In addition, the formation of air holes between calcium carbonate and the resin matrix was investigated from the phase morphology and interfacial behavior between the above constituents upon stretching using scanning electron microscopy. The tensile stress and the complex melt viscosity of the calcite filled (50%) polyethylene composites were higher than that of unfilled ones, implying that the reinforcing effect of calcium carbonate. The crack was initiated up to first 50% elongation along the transverse direction and the formation of air holes was originated by dewetting occurring through machine direction in the interface between calcium carbonate surface and HDPE. The propagation mechanism of the air hole formation was proposed to firstly originate by dewetting up to 300% elongation, and enlarged not only by breaking of a superimposed fibril structure, but also by merging effect air holes between fibrous resin matrix. However, the crack propagation was not observed at the very beginning elongation for the calcite filled LDPE and LLDPE systems. Less fibril structure was observed in LLDPE, then LDPE composites. The observed shape and the average size of the air holes were different from system to system. This sort of different interfacial behavior and mechanical properties may arise from different configuration of polyethylene.

Keywords: Interfacial behavior; Calcite filled polyethylene composites; Crack propagation

1. Introduction

Mineral fillers are often compounded into thermoplastic polymers not only to improve thermal, mechanical, and electrical properties, but also to reduce product cost. Calcium carbonate (calcite) plays an important role as reinforcing fillers in thermoplastic industry. It is well known that addition of such particulate significantly increases the viscosity of the compound. There are several studies reporting that viscosity of calcium carbonate filled thermoplastic composites increased [1–10], but in certain cases, it increased by several orders of magnitude at low shear rate, implying an occurrence of yield values. Few studies were also reported an observation of stretching flow for these compounds [2,4,7,8]. Similar rheological characteristics were observed at low strain rate when the compounds were filled with carbon black, calcium carbonate, and titanium dioxide.

Calcite whose chemical composition is $CaCO_3$ is an isotropic material, unlike other anisotropic minerals such as talc, mica, and clay containing two-dimensional layered silicate sheets. Compounding calcite into thermoplastic matrix has been studied from various researchers [4,6–14]. Dewetting property in particle filled polymer system is important as much as wetting in the interfacial point of view. Dewetting is widely used and demanding technique for baby diaper and sports wear industry. Calcite is known to disperse well in thermoplastic matrix. Coating calcite with chemicals were reported from various researchers [4,8,9,14] and stearic acid coated calcite has also been known to improve processibility of thermoplastic materials [4,8,9]. Calcite filled PE has been used for baby diaper due to their hydrophilic character [8,10,11–14]. Wang et al. [14] used a modifier consisting of carboxylated polyethylene and a

* Corresponding author.
E-mail address: sjchoe@inha.ac.kr (S. Choe).

0032-3861/02/$ - see front matter
PII: S0032-3861(02)00399-3

calcite grafted with acrylamide in high density polyethylene (HDPE) to improve mechanical property of the compound.

Ventilation property is one of the most important factors in manufacturing diapers and sports wear due to the process of dewetting. Thereby, an understanding of dewetting and air hole propagation by stretching a calcite filled polymers is of importance. There were some reports regarding on crack propagation [15–17]. In the blend of poly(methyl methacrylate) (PMMA) and polystyrene (PS), the crack propagation originated from PS particle was observed in the same direction after tensile treatment using transmission electron microscopy (TEM) [15]. On the other hand, for the blend of PS and PS/poly (butadiene) star block copolymer, the crack propagation was observed in various directions [16]. It was reported that the void network is responsible for crack propagation [17,18]. Baer's group extensively investigated for the post-failure analysis of a filled thermoplastic polyester and discussed by suggesting the five fracture modes based on the macroscopic stress–strain behavior [19–21]. However, there is no systematic research on dewetting and air hole propagation in the interface between treated calcite and polymer matrices under stretching. In addition, he suggested that these failures be characteristic of the fracture mode and would not depend on the filler type or filler content.

The objective of this research is to investigate the availability of control the size and the shape of the air hole by stretching the calcite filled HDPE, low density polyethylene (LDPE), and linear low density polyethylene (LLDPE) composites and to study the mechanism of the air hole formation stretching at various draw ratios. In addition, the rheological properties of the calcite filled HDPE, LDPE, and LLDPE composites were measured, which are related to the processibility.

2. Experimental

2.1. Materials

Polyolefins used in this study are HDPE, LDPE, and LLDPE supplied by SK Corporation, Korea. The compounds using calcium carbonate are HDPE/$CaCO_3$, LDPE/$CaCO_3$, and LLDPE/$CaCO_3$. Calcite (calcium carbonate) used in this study is stearic acid coated SST-40 supplied by DOWA Co., Japan and their average particle size and BET surface area are 1.1 μm and 4.8 m^2/g, respectively. The information of the materials used in this study is listed in Tables 1 and 2.

2.2. Compounding

A Brabender PL 2000 using a twin screw extruder was used for compounding calcite particle and HDPE, LDPE, and LLDPE with a 50:50 wt% ratio. Pre-mixed calcite and polyolefins were fed into extruder hopper and the compound materials extrudated through extruder die were passed in cold water bath of 20 °C, pelletized, then dried. Anti-oxidant and UV-stabilizer were also added to prevent from oxidation and UV absorption. A temperature gradient was maintained in the barrel of the extruder, that was at 190 °C in the feeding zone, at 210 °C in the compression zone, at 220 °C in the metering zone, and at 230 °C in the die end for HDPE system. The operation temperature of the extruder was ambient from sample to sample (HDPE at 230 °C, LDPE at 210 °C, and LLDPE system at 220 °C) and the screw was kept at 70 rpm (60 rpm for LDPE). The specimens used for this study were prepared using the composite materials mixed twice for better mixing.

2.3. Preparation of dumbbell bar and film

For the mechanical measurements, dumbbell bar shape specimens were prepared using the Carver laboratory hot press at 2×10^4 Pa and 200 °C. To compare the tensile properties between the unfilled polyethylene (pure polymer) and the calcite filled one, two types of ASTM, one is for composite type and the other is for pure polymer type, were used. The dimension of the dumbbell bar was $13 \times 3 \times 165$ mm^3 following the ASTM D638M-93 type M-I (dimension: $3 \times 15 \times 50$ mm^3 (grip distance)) for

Table 1
Characteristics of polyethylene used in this study

Olefin (grade name)	Density (g/cm^3)	MI (g/10 min)	HDT (°C)	Tensile strength (kg/cm^2)	Code
High density polyethylene (3300)	0.954	0.8	123	350	HDPE
Low density polyethylene (FB300)	0.919	3.0	90	120	LDPE
Linear low density polyethylene (FT810)	0.918	2.1	98	350	LLDPE

MI: melt index; HDT: heat distortion temperature.

Table 2
Properties of the calcite used in this study

Calcite (grade name)	Density (g/cm^3)	Particle size (μm)	BET area calculated (m^2/g)	Code (comment)
SST-40	2.9	1.1	4.8	Treated calcite

composite, and the ASTM D638M-93 type M-II (dimension: $2 \times 6 \times 25\ mm^3$ (grip distance)) for pure polymer. Film specimens were prepared using sheet extrusion using slit die having the dimension of $100 \times 1.5\ mm^2$, which was attached to the end of the extruder at temperatures same as that for the former die. Extruded sheet was pulled using take up device and the film thickness was maintained about 0.4 mm and cut into $15 \times 165\ mm^2$ (grip distance is 50 mm) following ASTM D882-97.

2.4. Characterization

2.4.1. Tensile test at different strain rates

The tensile stress of the dumbbell bar and films at yield and at break, and the elongation at break were measured using Instron 4301 at 20 °C and 30% humidity. Both ends of the specimen were firmly tightened by upper and lower grip. The initial gap separation distance was 50 mm and the strain rate (i.e. gap separation speed) was 50 and 5 mm/min for HDPE, LDPE and LLDPE system for dumbbell bar. In addition, to insure the effect of the strain rate on the mechanical properties, three different strain rates of 10, 50, and 500 mm/min were employed for HDPE, LDPE and LLDPE film systems filled and unfilled with calcium carbonate.

2.4.2. Tensile test at different draw ratios under constant strain rate

The slow strain rate at 5 mm/min and an initial gap separation at 2 mm were employed to carefully investigate the crack propagation and dewetting phenomena, then the draw ratio was varied from 50 to 500% depending on specimens to investigate the mechanism of the air hole formation.

2.4.3. Morphology

A Hitachi S-4300 scanning electron microscope (SEM) was used to obtain the image of the fractured surface, the stretched specimen surface and the particle agglomerate. The composite samples were fractured in liquid nitrogen and coated with platinum using a sputter coater. SEM microphotograph of each image was taken at 2000 magnification. The side surface of the dumbbell and film specimens was also studied after stretching the specimen at ambient strain rate and draw ratios.

2.4.4. Rheology

Complex melt viscosity of the compounds was measured using a Torsion Rheometer Mk III of Polymer Laboratory, Great Britain. After strain sweep experiment, the complex viscosity of the compounds was measured in a parallel plate ($D = 38$ mm) over a frequency range of $0.03–200\ s^{-1}$. The strain amplitude was maintained constant at 4% for all measurements. The shear stress for sinusoidal oscillatory flow experiments has the following form:

$$\sigma_{12}(t) = G'(\omega)\gamma \sin \omega t + G''(\omega)\gamma \cos \omega t = G^* \gamma \sin(\omega t + \delta) \tag{2.1}$$

where γ is the shear strain, G' is the storage modulus, G'' is the loss modulus, G^* is the complex modulus, ω is the frequency, and δ is the loss angle. The torque is related to the shear stress $\sigma_{12}(R)$ at the outer radius by

$$G'(\omega) = G^* \cos \delta = \frac{2MH}{\pi R^4 \theta} \cos \delta \tag{2.2}$$

$$G'(\omega) = G^* \sin \delta = \omega \eta' = \frac{2MH}{\pi R^4 \theta} \sin \delta \tag{2.3}$$

$$\eta^* = \sqrt{(\eta')^2 + (\eta'')^2} = \sqrt{\left(\frac{G''}{\omega}\right)^2 + (\eta'')^2} = \frac{G^*}{\omega} \tag{2.4}$$

The shear strain γ at the outer radius is $R\Delta\theta/H$, where M is the torque, R is the plate radius, H is the gap height, and θ is the shear angle.

3. Results and discussion

3.1. Tensile property

3.1.1. Pure polymer and the calcite filled composites at different strain rates with dumbbell bar

Before we study the tensile property of the composites, we examine the role of the stearic acid coated on the calcium carbonate. Then the result is the following. There is a strong chemical bonding between the polar group of the stearic acid ($C_{17}H_{35}COOH$) and the calcium carbonate (calcite) to form calcium stearate. Then the hydrophobic group ($-C_{17}H_{35}$) of the stearic acid attached to calcite particle is easily slip from the matrix polymer chain. Thus, the calcium stearate reduces the molecular friction resulting improvement of processing. Thereby, in this study, we only use the stearic acid treated calcium carbonate. In order to compare the mechanical properties between the calcite unfilled (pure polymer) and filled composites, tensile test of these two materials was carried out using two different types of specimens. Fig. 1(a) represents the stress–strain curves of HDPE, LDPE, and LLDPE pure polymers followed by the ASTM D638M-93 type M-I at a strain rate of 50 mm/min. The yield stress of HDPE is the highest at 24 MPa, then that of LLDPE and LDPE are the next order with 10.5 and 9.5 MPa, respectively. The elongation at break exhibited >1000, 480, and $>1000\%$, respectively ($>1000\%$ means that the observed elongation is larger than 1000% due to the machine limit since the machine only elongates the specimen for 20 min). In addition, Fig. 1(b) represents the stress–strain curves of pure polyethylene followed by the ASTM D638M-93 type M-II at a strain rate of 500 mm/min. The yield stress of HDPE, LDPE, and LLDPE is 27, 11, and 13 MPa, respectively. From this observation, the

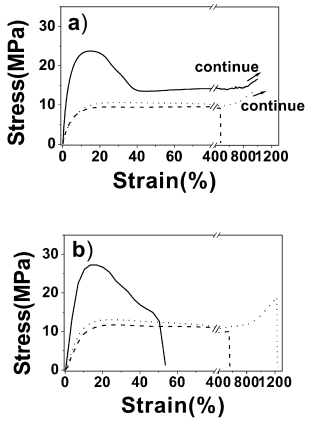

Fig. 1. Stress–strain curves of pure HDPE, LDPE, and LLDPE dumbbell for HDPE(—), LDPE(- - -), and LLDPE (···) by (a) ASTM (D 638M-93 type M-I), strain rate is 50 mm/min (b) ASTM (D 638M-93 type M-II), strain rate is 500 mm/min.

yield stress measured by the ASTM D638M-93 type M-I was slightly lower than by the ASTM D638M-93 type M-II due to lower strain rate and different specimen dimension. The elongation at break for HDPE, LDPE, and LLDPE are 53, 550, and 1250%, respectively, as seen in Fig. 1(b).

The comparison of the stress–strain curves for the calcite filled HDPE, LDPE, and LLDPE composites for dumbbell bar between 50 and 5 mm/min of strain rates are presented in Fig. 2(a)–(c), respectively. The maximum elongation at break for the calcite filled HDPE, LDPE, and LLDPE between 50 and 5 mm/min is 53 and 64, 12 and 16, and 34 and 42%, and the yield stress is 15, 9–10, and 10.5 MPa, respectively. From these figures, the lower the strain rate, the longer the elongation was observed, but no distinctive difference in yield stress between two different strain rates was observed. In particular, for the HDPE and LLDPE systems, after yielding, tearing was progressed near neck part until the dumbbell bar was broken. Since we are more interested in film specimen, the rest of the experiment was carried out using films.

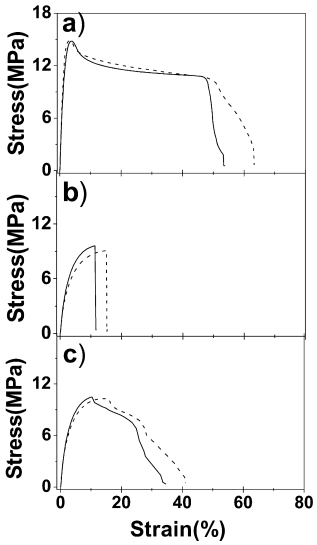

Fig. 2. Stress–strain curves of the calcite filled HDPE, LDPE, and LLDPE dumbbell at strain rates of 50 mm/min (—), and 5 mm/min (- - -). (a) HDPE (b) LDPE (c) LLDPE systems.

3.1.2. Films with different strain rates at 500, 50, and 10 mm/min

Fig. 3(a)–(c) represents the tensile stress–strain curves of the calcite filled HDPE, LDPE, and LLDPE films, respectively, measured at different strain rates of 500, 50, and 10 mm/min. For references, the stress–strain curves for the pure polymer measured at 500 mm/min was also presented. As seen in this figure, the elongation at break of the pure polymer HDPE, LDPE, and LLDPE was 850, 720, and >1000%, respectively. In addition, the elongation at break for the calcite filled HDPE, LDPE and LLDPE composites exhibited 760, 350, and 510% at strain rate of 500 mm/min as shown in Fig. 3(a)–(c). At a strain rate of 50 mm/min, the HDPE composite exhibited the highest elongation at a break of 840%, then LLDPE composite at 650%, and then LDPE one at 240%. As the strain rate lowered to 10 mm/min, HDPE, LDPE and LLDPE composites exhibited >400, 160, and >400% (>400% means that the observed elongation is larger than 400% due to the machine limit since the machine only elongates the specimen for 20 min). A surprising observation in the LDPE system was that the higher the strain rate, the longer the elongation at break was observed from 160 to 240 and 350%. On the other hand, for the HDPE and LLDPE systems, the higher the strain rate, the shorter was the elongation at break, which is in contrast to the LDPE system. Since LDPE exhibits high molecular weight with broad molecular weight distribution due to long and short chain branching, the higher the strain rate, the longer the

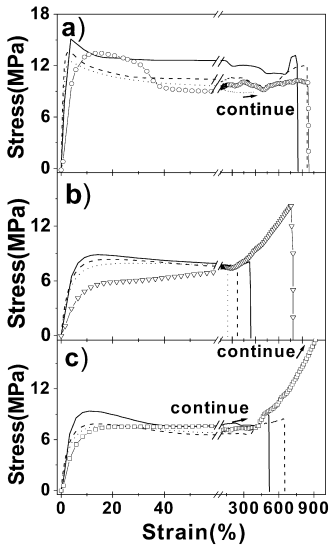

Fig. 3. Stress–strain curves of the calcite filled film systems at strain rates of 500 mm/min (—), 50 mm/min (- - -), and 10 mm/min (···). ○, ▽, □ symbols represent the pure polymers at 500 mm/min (a) HDPE (b) LDPE (c) LLDPE.

elongation at break was induced, which may be an important factor for better processibility.

As the strain rate decreased from 500, 50 to 10 mm/min, the yield stress decreased from 15 to 12.5 MPa for HDPE composite, from 9 to 8 MPa for LDPE, and from 9.5 to 7.5 MPa for LLDPE system. When we compare the yield stress and the elongation at break between unfilled and calcite filled films at 500 mm/min, the yield stress of the latter systems relatively increased, but the elongation at break decreased. This implies that the inclusion of calcite in HDPE, LDPE and LLDPE provides a reinforcement effect, but poor flexibility and reduced toughness.

Modulus, yield stress, and elongation at break of the calcite filled HDPE, LDPE, and LLDPE films are plotted all together in Fig. 4. Although there is no consistency between three different strain rates, HDPE system is relatively the highest in modulus, yield stress, and elongation at break, then come LLDPE and LDPE systems in the order. For modulus, the strain rate at 50 mm/min exhibited the highest value, then 10 and 500 mm/min. For elongation at break, strain rate of 10 mm/min exhibited the highest value, then 50 and 500 mm/min.

3.2. Rheology

3.2.1. Strain sweep and melt viscosity

The complex melt viscosity (η^*) of unfilled and the calcite filled HDPE, LDPE, and LLDPE composites at 10 (rad/s) and at 240 °C is plotted as a function of strain sweep from 0.25 to 16% in Fig. 5(a)–(c), respectively. As seen in this figure, the complex viscosity of the calcite-filled system was constant with the strain sweep and was higher than that of the unfilled system. As calcite particle distributed between polymer

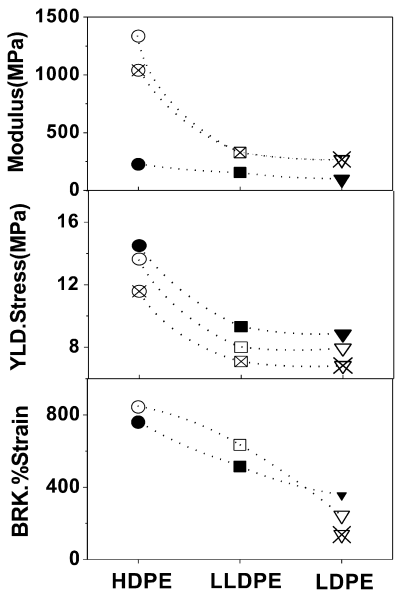

Fig. 4. Modulus, yield stress, and elongation of the calcite filled HDPE, LDPE, and LLDPE film. Symbols represent the different strain rates: solid (500 mm/min), open (50 mm/min), and cross (10 mm/min).

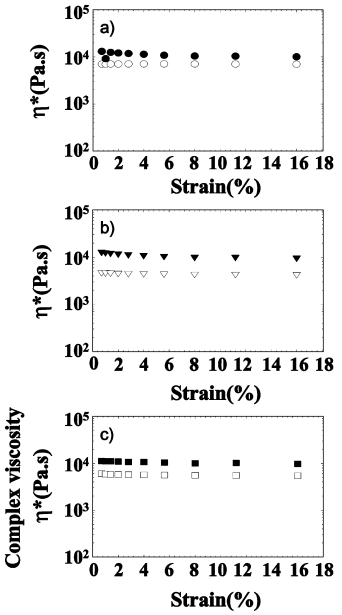

Fig. 5. Complex melt viscosity as a function of strain sweep of (a) HDPE, (b) LDPE, (c) LLDPE system at 240 °C and share strain rate $\omega = 10\ s^{-1}$. Open symbol (pure polymers), and solid symbol (calcite composite).

chains, the mobility of the polymer chain restricted by the filler, then the modulus of the composite increased, but processibility decreased. Fig. 6 shows the complex melt viscosity of the calcite unfilled and filled HDPE, LDPE, and LLDPE systems at a frequency range from 0.03 to 200 rad/s. As the oscillation rate increased, the viscosity level of each system decreased due to shear thinning effect. In addition, calcite filled materials exhibited relatively higher viscosity than that of the unfilled ones due to the increase in contacting area between calcite surface and polymer. This result agrees well with the tensile property, which implies that the calcite filled polyethylene composites exhibit reinforcing effect due to an addition of calcium carbonate. At a low frequency range ($\omega = 0.03$ rad/s), the viscosity of HDPE system was the highest, then the LLDPE and LDPE systems, however, at a high frequency (200 rad/s), the LLDPE system exhibited the highest viscosity among three systems. This may arise from the different degree of branching, molecular weight and the molecular weight distribution of each polymer system.

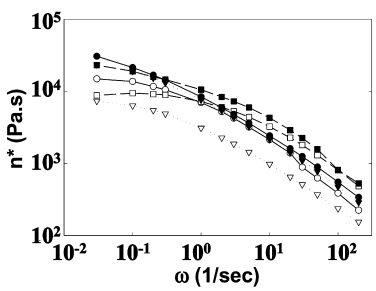

Fig. 6. Complex melt viscosity of the calcite unfilled and filled HDPE, LDPE and LLDPE systems as a function of frequency; –○– (pure HDPE), –▽– (pure LDPE), –□– (pure LLDPE); ···●··· (filled HDPE), ···▼··· (filled LDPE), ···■··· (filled LLDPE).

3.2.2. Storage modulus (G') and loss modulus (G'') cross-over

After strain sweep at a frequency rate of 10 rad/s, storage modulus (G') and loss modulus (G'') were measured at 4% strain and 200 °C. We observed the cross-over point of G' and G'' of each system as shown in Fig. 7. Calcite filled LDPE composite exhibited cross-over at low frequency region at 1.3 rad/s, then HDPE at 2.1 rad/s, and then LLDPE at 7.3 rad/s. The shift of cross-over point to higher frequency region may due to lower G' or higher G''. Thus calcite filled LDPE system seems to have higher molecular weight or low molecular weight distribution while calcite filled LLDPE composite seems to show low molecular weight or high molecular weight distribution. HDPE/$CaCO_3$ composite is in between LDPE and LLDPE systems.

3.3. Morphological observation

Fig. 8 presents the SEM photographs of various parts of the calcite filled HDPE films stretched at a strain rate of 5 mm/min and an initial gap distance of 10 mm. In this figure, (a) exhibits the side part of the film before stretching, (b) exhibits the fracture part before stretching, (c) shows the neck part after stretching, then (d)–(f) represent the side part of the specimen after stretching at different draw ratios 100, 200, and 500%, respectively. Although there is no

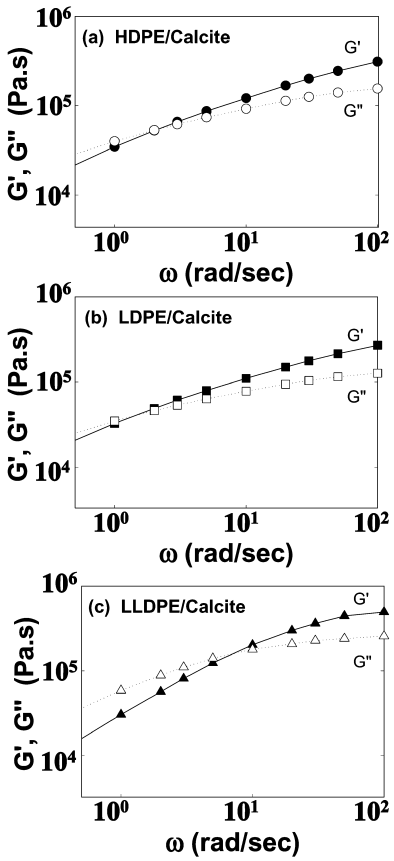

Fig. 7. Storage modulus (G') and loss modulus (G'') cross-over for the (a) HDPE, (b) LDPE, and (c) LLDPE composites.

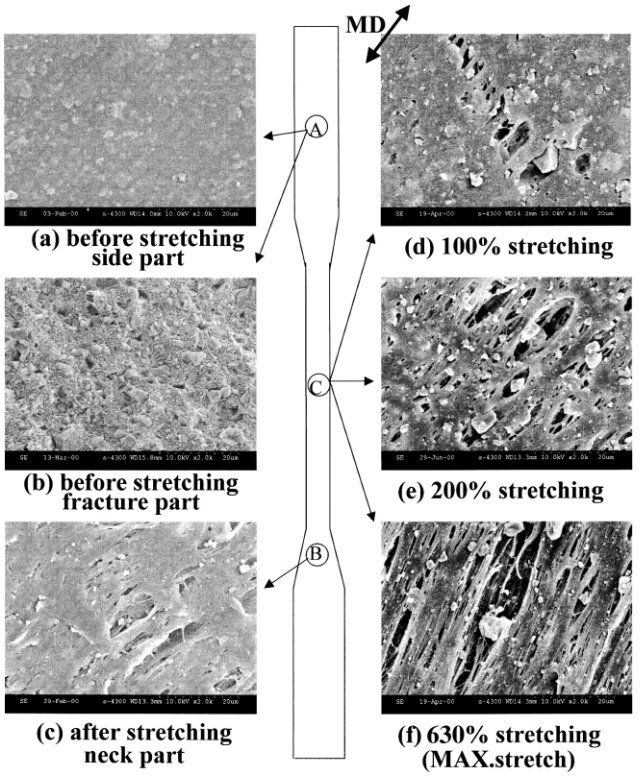

Fig. 8. (a)–(f) SEM photograph of the calcite filled HDPE for various draw ratios including neck part at 5 mm/min with an initial grip distance of 10 mm.

specific observation in Fig. 8(a), dewetting is observed from the fractured interface between the calcite surface and polymer as seen in Fig. 8(b). In Fig. 8(c), the neck part is torn due to stretching, followed by a formation of air hole with a fibril structure in HDPE matrix. When the draw ratio reached 100% in Fig. 8(d), crack propagation was observed along the transverse direction (TD) and a simultaneous dewetting was observed in the interface between the calcite and HDPE resin along the machine direction (MD). As the draw ratio increased to 200% as seen in Fig. 8(e), the air holes are formed mostly by the dewetting of the calcite particles along the MD and enlarged. However, at 630% elongation as seen in Fig. 8(f), the air hole formation is merged and dominated by the breaking of a superimposed fibril structure.

In Fig. 9, in the calcite filled LDPE system, there was no big difference between HDPE and LDPE systems in Fig. 9(a), which exhibits the side part of the film specimen before stretching. However, there is a slight difference in Fig. 9(b) and (c), which shows the fracture part before stretching and the neck part of the specimen, respectively. In LDPE system seen in Fig. 9(b), the calcite seems to be more wetted in LDPE matrix than as seen in HDPE in Fig. 8(b). In addition, in Fig. 9(c), small portion of crazing is formed between the weakened region between the calcite and the LDPE resin. The big difference between HDPE and LDPE composites is prominent, when they are stretched as seen in Fig. 9(d)–(f),

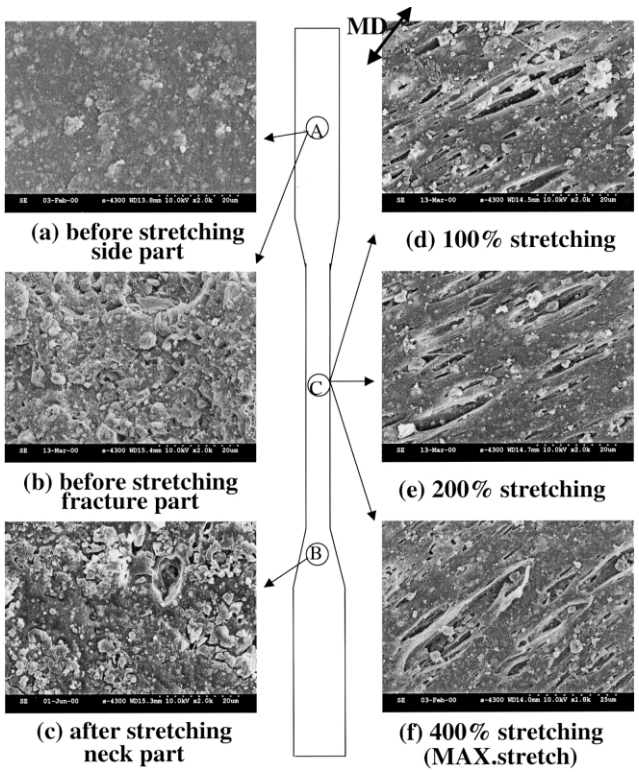

Fig. 9. (a)–(f) SEM photograph of the calcite filled LDPE for various draw ratio including neck part at 5 mm/min with an initial grip distance of 10 mm.

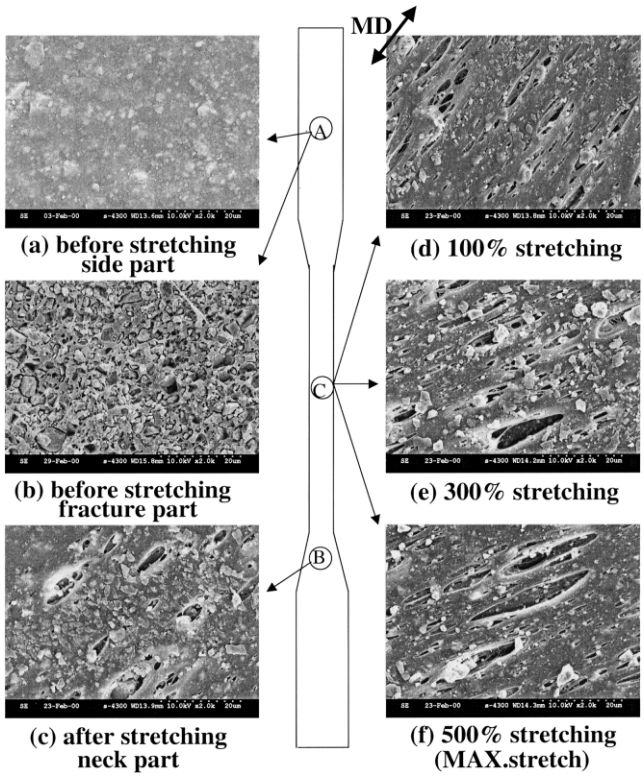

Fig. 10. (a)–(f) SEM photograph of the calcite filled LLDPE for various draw ratios including neck part at 5 mm/min with an initial grip distance of 10 mm, but observed length is 2 mm.

the calcite particles seem to migrate above the film surface. The air hole was formed and enlarged due to dewetting, but there is no observation of tearing or fibril structure up to 300% stretching.

For the calcite filled LLDPE composite as seen in Fig. 10, Fig. 10(a) and (b) seems to be much similar to HDPE system. However, in Fig. 10(c), dewetting was observed more prominently in this system, then the formation of air hole was accelerated with draw ratio. We observed the combined characteristics of LDPE and HDPE in LLDPE system. That is the migration of the calcite particles above the film matrix similar to that of LDPE, and the formation of air hole along the MD and an observation of fibril structure at high draw ratio (500%) similar to HDPE. Thus the morphological behavior of LLDPE composite is similar to that of LDPE up to 200% draw ratio, but similar to that of HDPE one at 500% draw ratio.

In order to quantitatively investigate the crack propagation and a formation of air hole, we marked a very short length of specimen (2 mm) as an initial gap distance and observed the interfacial and morphological behavior by stretching at various draw ratios. SEM photographs of the calcite filled HDPE, LDPE, and LLDPE films at various draw ratios at constant strain rate 5 mm/min and a gap distance 2 mm are shown in Figs. 11–13, respectively. For

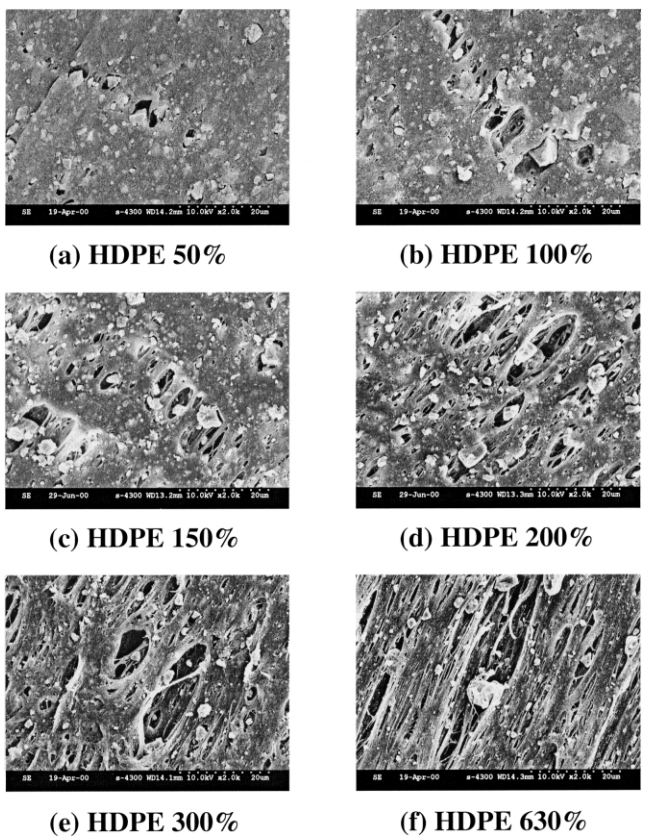

Fig. 11. (a)–(f) SEM photograph of 50, 100, 150, 200, 300, and 500% draw ratio on the calcite filled HDPE at 5 mm/min with an initial grip distance of 10 mm, but observed length is 2 mm.

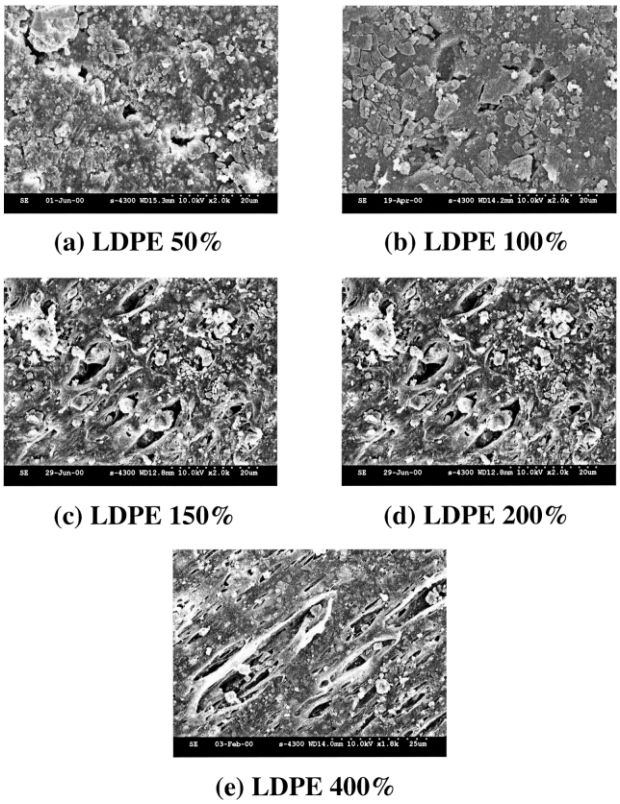

Fig. 12. (a)–(f) SEM photograph of 50, 100, 150, 200, and 300% draw ratio on the calcite filled LDPE at 5 mm/min with an initial grip distance 10 mm, but observed length is 2 mm.

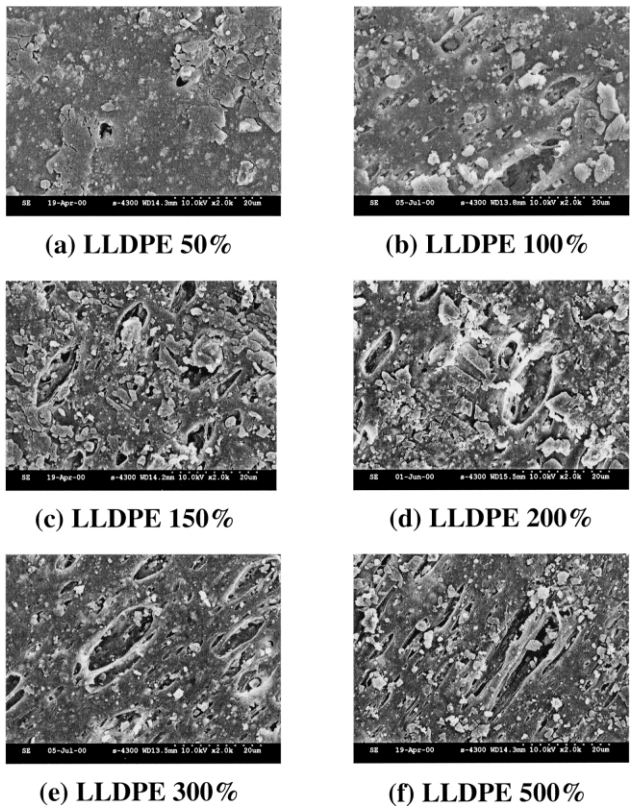

Fig. 13. (a)–(f) SEM photograph of 50, 100, 150, 200, 300, and 400% draw ratio on the calcite filled LLDPE at 5 mm/min with an initial grip distance of 10 mm, but observed length is 2 mm.

HDPE system, Fig. 11(a)–(f) presents the side part of the stretched film as given in each figure at 50, 100, 150, 200, 300, and 630% draw ratios, respectively. Crack was initiated at 50% draw ratio as seen in Fig. 11(a), then it propagated along the TD of the film up to 100%, and enlarged at 150% draw ratio. In addition, dewetting and a simultaneous formation of air holes took place at the interface between the calcite surface and the polymer, where the low interfacial force was formed upon 50% draw ratio. As the specimen stretched up to 200%, the air holes became larger and larger due to dewetting of the calcite particles and emerged by breaking the fibril structure of HDPE. As draw ratio increased further (300 and 630%), the depth and the size of the air holes are enlarged mostly due to the merging of the other air holes by breaking the fibril structure. At 630% draw ratio, the composite surface was composed with fully fibrillated structure along the MD as seen in Fig. 11(f).

In Fig. 12(a) at 50% draw ratio for LDPE system, we observed two major phenomena; a migration of the calcium carbonate over the film surface and a formation of small air hole due to dewetting of the calcite particle from the LDPE matrix. At 100% draw ratio in Fig. 12(b), the only difference is the size of the average air hole. At 150% draw ratio as seen in Fig. 12(c), the propagation of air holes between the calcite particles and the resin matrix was taken place due to the weakened interfacial forces. At 300% draw ratio in Fig. 12(e), the size of the air hole enlarged due to sorely dewetting of the calcite particles, but no fibril structure was observed as we have seen in the HDPE system.

For LLDPE system as seen in Fig. 13(a)–(f), we observed a similar behavior to that of the LDPE system from 50 to 300% draw ratio. In Fig. 13(a) with 50% draw ratio, the formation of some small air holes by dwetting of the calcite particles from the LLDPE matrix was observed, and this may arise from weakened interfacial adhesion between two constituents. At 100% draw ratio, dewetting is more prominent between the calcite and LLDPE, then the average size and the number of the air holes augmented as the draw ratio increased up to 300%. Upon further stretching at the maximum draw ratio of 500%, fibrous structure as seen in HDPE system, is also observed in LLDPE system.

From the morphological observations in the calcite filled HDPE, LDPE, and LLDPE composites as seen in Figs. 11–13, we can propose the propagation mechanism of air hole formation. As seen in Fig. 14(a), the formation of air hole was originated by dewetting behavior between the calcite and the polyethylene matrix upon stretching. Then as seen in Fig. 14(b), the air hole enlarged due to the continuous elongation up to a certain draw ratio. Finally, when the specimen was stretched further in Fig. 14(c), the size of the air hole was dominated not only by the broken fibrous structure (in Fig. 14(c); lower part), but also by the merging effect of the air holes (in Fig. 14(c); upper part).

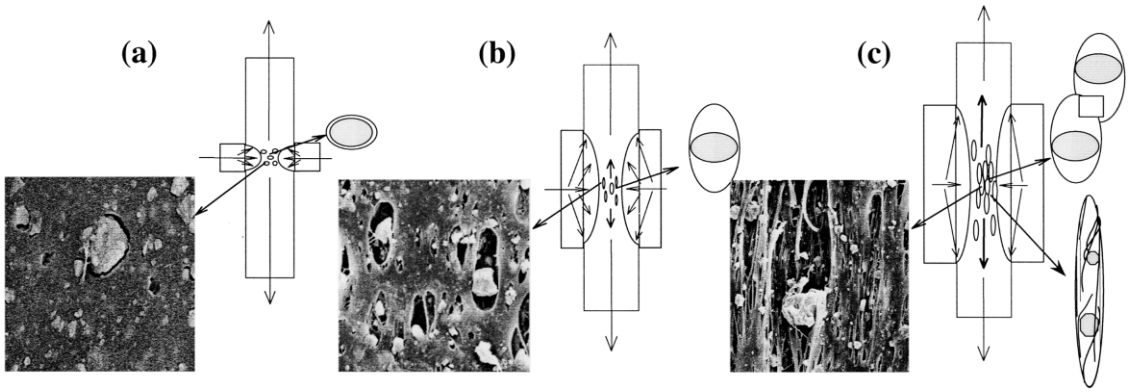

Fig. 14. The proposed mechanism of an air hole formation. (a) air hole formation due to dewetting, (b) enlargement of air hole upon further stretching, and (c) air hole enlargement by merging effect between the air holes and broken fibrous structure of resin matrix.

4. Conclusions

Mechanical properties and complex melt viscosity of the calcite (calcium carbonate: $CaCO_3$) unfilled and calcite filled polyethylene using HDPE, LDPE, and LLDPE composites were studied using dumbbell bar and film specimens. In addition, the mechanism of the formation of air holes was proposed from the phase morphology and interfacial behavior between the calcite and the resin matrix upon stretching using SEM. Tensile stress, modulus, elongation at break were compared to study the role of calcium carbonate at different draw ratios and strain rates using calcite filled polyethylene systems. The tensile stress and the complex melt viscosity of the calcite filled polyethylene composites were higher than that of unfilled ones, implying that the reinforcing effect of the calcium carbonate. The crack was initiated up to first 50% elongation along the TD and the formation of air holes was originated by dewetting occurring through MD in the interface between the calcium carbonate surface and the HDPE matrix. The air hole enlarged up to 300% elongation due to dewetting of the calcite, but then enlarged by a breaking of a superimposed fibril structure and merging effect of the preformed various sizes of air holes upon further stretching. However, the crack propagation was not observed for the calcite filled LDPE and LLDPE systems. Less fibril structure was observed in LLDPE, then LDPE composites. The observed shape and the average size of air holes were different from system to system, which may have arisen from the different mechanism of the formation of air holes. This sort of different interfacial behavior and mechanical properties may arise from different configuration of polyethylene.

Acknowledgments

This work has been supported by SK Corporation. In particular, Dr Kwang Jea Kim and Dr Patit P. Kunda thank Korea Research Foundation and Inha University for giving a chance for him to work at Inha University as a post-doc by Korea Research Foundation Grant (KRF-99-E013).

References

[1] Kataoka T, Kitano T, Sasahara M, Nishijima K. Rheol Acta 1978;17:149.
[2] Tanaka H, White JL. Polym Engng Sci 1980;20:949.
[3] White JL, Czarnecki L, Tanaka H. Rubber Chem Technol 1980;53:823.
[4] Tanaka Y, White JL. J Appl Polym Sci 1983;28:1481.
[5] Li L, White JL. Rubber Chem Technol 1996;69:628.
[6] Kim KJ, White JL. J Non-Newtonian Fluid Mech 1996;66:257.
[7] Kim KJ, White JL. Polym Engng Sci 1999;39(11):2189.
[8] Kim KJ. Dissertation. Rheology, processing, and characterization of isotropic, anisotropic, and mixed particle filled polymer system. University of Akron; 1998.
[9] Kim KJ, White JL, Choe SJ, Dehennau C. Accepted in J Appl Polym Sci.
[10] Harrington EA. Am J Soc 1927;13:467.
[11] Chacko VP, Karasz FE, Farris RJ. Polym Engng Sci 1982;22:968.
[12] Chacko VP, Farris RJ, Karasz FE. J Appl Polym Sci 1983;28:2701.
[13] Banhegyi G, Karasz FE. J Polym Sci: Polym Phys 1986;24:209.
[14] Wang Y, Lu J, Wang G. J Appl Polym Sci 1997;64:1275.
[15] Trent JS, Scheinbeim JI, Couchman PR. Macromolecules 1983;16:589.
[16] Gebizlioglu O, Argon A, Cohen R. Polymer 1985;26:519.
[17] Woodward AE, Morrow DR. J Polym Sci A2 1969;7:1651.
[18] Woodward AE. Atlas of polymer morphology. Munich: Hanser; 1988.
[19] Bazhenov S, Li JX, Hiltner A, Baer E. J Appl Polym Sci 1994;52:243.
[20] Li JX, Silvestein M, Hiltner A, Baer E. J Appl Polym Sci 1994;52:255.
[21] Li JX, Hiltner A, Baer E. J Appl Polym Sci 1994;52:269.